International Journal of Heat and Mass Transfer 53 (2010) 1283–1289

Contents lists available at ScienceDirect

International Journal of Heat and Mass Transfer

journal homepage: www.elsevier.com/locate/ijhmt

Effect of residual gas on the dynamics of water adsorption under isobaric stages of adsorption heat pumps: Mathematical modelling

B.N. Okunev [a,*], A.P. Gromov [a], V.L. Zelenko [a], I.S. Glaznev [b], D.S. Ovoshchnikov [b], L.I. Heifets [a], Yu.I. Aristov [b]

[a] Moscow State University, Chemical Department, Vorobievi Gori, Moscow, Russian Federation
[b] Boreskov Institute of Catalysis, Pr. Lavrentieva, 5, Novosibirsk 630090, Russian Federation

ARTICLE INFO

Article history:
Received 2 November 2009
Received in revised form 7 December 2009
Accepted 8 December 2009
Available online 14 January 2010

Keywords:
Mathematical modelling
Residual gas
Coupled heat and mass transfer
Adsorption kinetics
Selective water sorbents
Adsorption chiller

ABSTRACT

A mathematical model of the coupled heat and mass transfer in an adsorbent layer was developed to study the effect of a non-adsorbable gas (air, hydrogen) on kinetics of water adsorption on loose grains of the composite adsorbent SWS-1L (silica modified by calcium chloride). The adsorbent monolayer was placed on the surface of an isothermal metal plate at $T = 60$ °C and equilibrated with the mixture of water vapor at constant $P = 10.3$ mbar in the presence of the non-adsorbable gas at a variable partial pressure $P_A = 0.06–14.3$ mbar. After that the metal plate is subjected to a temperature drop down to 35 °C that initiates water adsorption. It is shown that the adsorption of water causes effective gas sweeping to the surface where it was accumulated as a gas-rich layer. This results in dramatic slowing down of the adsorption and heat transfer processes.

© 2009 Elsevier Ltd. All rights reserved.

1. Introduction

Adsorptive heat transformation (AHT) based on solid adsorption systems has received much attention in recent years as an alternative to conventional compression systems using CFC [1–4]. In order to be competitive with compression refrigerators the specific power of the AHT units has to be improved. A non-adsorbable gas can greatly affect the rate of adsorption and, hence, the AHT specific power. Indeed, an important feature of AHT with water as a working fluid is low pressure during isobaric ad- and desorption phases. Because of this, the presence of even little amount of air (or any other non-adsorbable gas) can significantly affect the AHT performance. This phenomenon is well-known from practical utilization of heat and mass transfer apparatuses. Chlorine production is accompanied by the generation of a modicum of hydrogen which little by little is accumulated in a heat exchanger-condenser. This reduced both the average chlorine concentration and increases the hydrogen concentration in the vicinity of condenser surface [5]. This gradual accumulation is caused by a Stephan flux [6,7], which effectively sweeps hydrogen to the condenser surface. In [7], the authors revealed the reduction of heat transfer in a granulated adsorbent layer in the presence of residual air. It was supposed that this effect can significantly reduce the performance of AHT. In practice a residual gas can present inside evacuated AHT equipment: air due to leakage or desorption, while hydrogen due to corrosion. Detailed study of the mentioned reduction was performed in [8,9]. In [8], the effect of a non-adsorbable gas (air) on kinetics of water adsorption on loose grains of the composite adsorbent SWS-1L (silica modified by calcium chloride) (grain size 0.8–0.9 and 1.4–1.6 mm) was studied. The adsorbent grains were placed on the surface of isothermal metal plate at $T = 60$ °C and equilibrated with the mixture of water vapor at $P_{H2O} = 10.3$ mbar and air at a certain partial pressure P_A. After that the metal plate was subjected to a temperature drop down to 35 °C at almost constant pressure over the grains. Reduction of the adsorption rate was revealed even at the partial pressure of residual air P_A as low as 0.05 mbar. At $P_A > 0.4$ mbar, the kinetic curves were near-exponential and the characteristic adsorption time τ increased as $\tau = \tau_0 + BP_A$, where $B = 700 \pm 50$ s/mbar. Desorption stage was less affected by the residual air. The specific power released during adsorption process was estimated as a function of the amount of residual gas. In [9], the study of this effect was extended over two adsorbents promising for adsorption chilling: silica Fuji type RD and FAM-Z02. The rate of adsorption by the loose grains of Fuji silica RD was found to be less sensitive to the presence of residual air than for SWS-1L. The characteristic time $\tau_{0.8}$ linearly increased with the rise in P_A with the slope $B = 250 \pm 6$ s/mbar. FAM-Z02 demonstrated intermediate behavior with $B = 590 \pm 45$ s/mbar.

* Corresponding author. Tel.: +7 495 939 46 49; fax: +7 495 939 33 16.
E-mail address: okunev@tech.chem.msu.ru (B.N. Okunev).

0017-9310/$ - see front matter © 2009 Elsevier Ltd. All rights reserved.
doi:10.1016/j.ijheatmasstransfer.2009.12.040

Nomenclature

C	concentration (mole/m^3)
c_p	effective heat capacity (J/(kg K))
D_W	efficient water diffusivity (m^2/s)
ΔH	heat of adsorption (J/mole)
J	molar flux (mole/(m^2 s))
L	characteristic diffusional length (m)
m	mass (kg)
N	uptake (mole H_2O/mole $CaCl_2$)
P	pressure (mbar)
R_p	grain radius (m)
R	universal gas constant (J/(mole K))
t	time (s)
T	temperature (K)
u	convective speed of the gas mixture (m/s)
V	volume (m^3)
x	weight fraction of the salt (kg/kg)
z	spatial coordinate

Greek symbols

α_p	heat transfer coefficient (W/(m^2 K))
ε	grain porosity
ν	dimensionless adsorption
λ	coefficient of heat conductivity (W/(m K))
μ	mass (kg/kmole)
ρ	density (kg/m^3)

Subscripts

0	initial value
a	air
A	residual gas
W	water vapor

The formation of the gas-rich layer in the vicinity of grain surface is a complex process that is influenced by coupled heat and mass transfer between the grain and gas phase as well as inside the grain. In this paper we report a mathematical model which describes the origin of the Stephan flux, the formation and temporal evolution of the gas-rich layer near the surface of the composite sorbent SWS-1L. The description of water sorption process inside the grain was performed in much the same way as in [10]. It was our aim in this work to calculate the evolution of temperature, pressure and concentration of the adsorbed water as a function of time t and the distance r from the grain center. When possible, the calculated values were compared with those experimentally measured in [8] (for residual air) or in this work (for residual hydrogen).

2. Experimental

To measure the dynamics of water sorption on SWS-1L in the presence of hydrogen, we used the same methodology (the so-called large temperature jump (LTJ) method [11]) and equipment as it was carefully described in [8] for the residual air. The adsorbent grains were placed on the surface of an isothermal metal plate at $T = 60$ °C and equilibrated with the mixture of water vapor at $P = 10.3$ mbar and air (hydrogen) at a certain partial pressure P_A between 0.06 and 14.3 mbar. After that the metal plate was subjected to a temperature drop down to 35 °C at almost constant pressure over the grains. The data of the pressure evolution P(t) required for calculating the water uptake $m(t)$ were recorded each 1 s by a data acquisition system. Dimensionless uptake was calculated as $\nu = m(t)/m(\infty)$.

The tested adsorbent SWS-1L was prepared by a silica KSK impregnation with a saturated aqueous solution of $CaCl_2$ at $T = 25$ °C. The salt content amounted to 33.7 wt% (dry base). The average pore diameter of SWS-1L was 15 nm. Grain sizes of the sample was selected as 1.6–1.8 mm. Typical weight of the dry sample was 0.420–0.425 g that corresponded to a one layer of loose grains covering the metal plate.

3. Sorption dynamics in the presence of hydrogen

After initiating the holder cooling, its temperature reached the final temperature within approximately 1 min, while the pressure reduction was slower and lasted some tens minutes or even hours (Fig. 1). At any P_A, the kinetic curves of water sorption were near-exponential over the whole range of uptake so that $m(t) = m_0 + (m_f - m_0)[1 - \exp(-t/\tau)]$ that is similar to the sorption dynamics in the presence of air [8]. A thorough look at the curves reveals that the experimental uptake is slightly larger than exponential at short and long times, and somewhat smaller – at intermediate times. The difference does not exceed 0.03 and increases at elevated P_A (Fig. 1). Interestingly, that in the presence of air no deviation was observed and the uptake curves were very close to exponential [8].

The characteristic time of sorption increased as $\tau = \tau_0 + BP_A = 261$ s + 177 s/mbar, where τ_0 is the characteristic time in a pure vapor ($P_A = 0$) and B is the slope that characterizes an impact of residual gas (Fig. 2). This figure demonstrates that the effect of residual hydrogen is less dramatic as compared with air, and the ratio of the slopes $B(\text{air})/B(H_2)$ is equal to 3.64. This ratio is close to the ratio of effective diffusivities (cm^2/s) in the binary mixture "air–vapor"

$$D_a = 292/(P_W + P_A),$$

and "hydrogen–vapor"

$$D_h = 1136/(P_W + P_A),$$

where P_W is the vapor partial pressure (in mbar), equal to $D_h/D_a = 3.89 \approx (\mu_a/\mu_h)^{1/2}$, where μ_a and μ_h are the molecular masses of air and hydrogen [12].

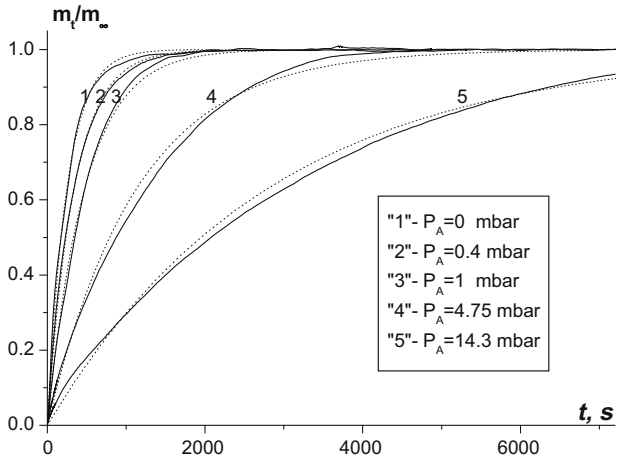

Fig. 1. Dimensionless uptake curves of water sorption on SWS-1L at various partial pressures of hydrogen (dashed lines). Solid lines give an exponential approximation.

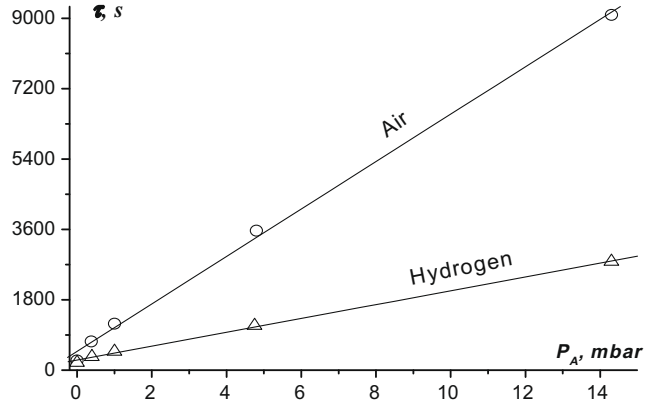

Fig. 2. Characteristic sorption time τ vs. air and hydrogen partial pressure for SWS-1L loose grains. Lines – linear approximation.

Higher diffusivity of hydrogen leads to faster molecular motion against the concentration gradient that promotes destroying of the gas-reach layer which has been formed by the Stephan flux. As a result of these randomizing and ordering processes, the effect of slowing down the water sorption becomes less dramatic than in the presence of air.

Desorption stage was less affected by the residual gas because the hydrogen-rich layer did not form on this case. The desorption rate was limited by the intraparticle vapor diffusion or the dissipation of adsorption heat from the grain external surface.

4. Description of the mathematical model

This model represents the process of coupled heat and mass transfer in the adsorbent grains jointed with convective mass transfer in the gas phase in the presence of a non-adsorbable gas. We considered a monolayer of loose spherical adsorbent grains of radius R_p, which are located on the metal support. At $t = 0$, the grains are in equilibrium with water vapor at the initial temperature T_0 and pressure $P_0 = P_W + P_A$, where P_W and P_A are the partial pressures of vapor and air, respectively. The support is subjected to a step-wise cooling from T_0 down to the final temperature T_f, which stimulates the process of vapor adsorption. We assumed that the gas in the vicinity of the support acquires the same temperature T_f in a very short time. In this case the heat flux q from the grain surface can be written as $q = \alpha_p(T_f - T(R_p, t))$, where α_p is the effective heat transfer coefficient that accounts for the integrated exchange of heat between the grain, metal support and gas phase, $T(R_p, t)$ is the temperature of particle surface. The larger the air pressure P_A is the more valid is this assumption. Because of this flux, the grain is cooling. Its temperature $T(r, t)$ depends on the heat transfer inside the grain and from the grain to the support and surrounding gas as well as on the adsorption rate. The vapor adsorption starts, and it creates the convective flux of vapor towards the grain (layer) surface (the Stephan flux). Hence, the evolution of water uptake results from a set of complex interdependent processes inside the grain (diffusion, adsorption, and heat release) and between the grain and the gas phase (convective diffusion of the both components).

For describing the water adsorption in the single grain in the presence of residual air we have modified the model developed in [8,11]. Combined heat and mass transfer in a single adsorbent grain in the presence of air was described by the following system of differential equations:

(a) Temperature $T(r, t)$ in the adsorbent grain changes due to the heat released during the water adsorption and the heat transfer in the grain:

$$\rho_s c_p(T, N, x)\frac{\partial T}{\partial t} - \rho_s \Delta H \frac{x}{\mu_{salt}}\frac{\partial N}{\partial t} = \frac{\lambda}{r^2}\frac{\partial}{\partial r}\left(r^2\frac{\partial T}{\partial r}\right), \qquad 0 < r < R_p, \tag{1}$$

where ρ_s is the grain density, $c_p(T, N, x)$ is the effective heat capacity of the grain [13], $N(T, P_w)$ [mole H_2O/mole salt] is the equilibrium uptake at temperature T and pressure P_w being calculated by approximation equations reported in [14], ΔH is the heat of water sorption, χ is a mass fraction of the salt (calcium chloride) in the composite adsorbent, μ_{salt} is the salt molar mass, λ is the heat conductivity of adsorbent grain.

The relevant initial and boundary conditions are:

At $t = 0$ the grain temperature is constant and equal to the initial temperature in the system T_0

$$T(r, 0) = T_0.$$

The heat flux in the grain center

$$\frac{\partial T(0, t)}{\partial r} = 0.$$

The heat flux through the grain surface

$$\alpha_p(T_f - T(R_p, t)) = \lambda_p \frac{\partial T(R_p, t)}{\partial r}.$$

(b) Concentration of the adsorbed water $C_W(r, t)$ in the grain changes as a result of adsorption and diffusion

$$\frac{\partial C_W}{\partial t} = \frac{D_W}{r^2}\frac{\partial}{\partial r}\left(r^2\frac{\partial C_W}{\partial r}\right) - \frac{\rho_s x}{\mu_{salt}\varepsilon}\frac{\partial N}{\partial t}, \tag{2}$$

where D_W is the water diffusivity in the grain.

The initial and boundary conditions are the initial concentration is constant and equal to

$$C_W(r, 0) = \frac{P_W(0)}{RT_0},$$

due to a spherical symmetry the derivative

$$\frac{\partial C_W(0, t)}{\partial r} = 0.$$

(c) The mass of air inside the grain is negligible with respect to its mass in the gas phase.

(d) The mass transfer resistance from the gas side is described by the following balance equations of the convective diffusion of each component:

$$\begin{aligned} &\frac{\partial C_W}{\partial t} + \frac{\partial J_W}{\partial z} = 0, \\ &\frac{\partial C_A}{\partial t} + \frac{\partial J_A}{\partial z} = 0, \\ &0 < z < L, \end{aligned} \tag{3}$$

where z is a dimensionless length, L is the length characteristic for a particular experimental set-up. The mass fluxes J_W and J_A consist of the convective and diffusional terms

$$J_A = C_A u - D_{WA} C_{WA}\frac{\partial x}{\partial z}, \quad J_W = C_W u + D_{WA} C_{WA}\frac{\partial x}{\partial z},$$

where $x = \frac{C_A}{C_{WA}}$ is a molar fraction of residual gas in the gas phase, $u(z, t)$ is a convective speed of the gas mixture. Coefficient of the interdiffusion D_{WA} (m^2/s) was calculated using an empirical equation for the binary mixtures "air–vapor" and "hydrogen–vapor" [8] (see above).

The initial and boundary conditions for Eq. (3) are at $t = 0$ the initial content of the gas mixture is known from the experiment, the vapor flux through the outer grain surface is equal to the vapor flux towards the grain center:

$$D_W \frac{\partial C_W(R_p, t)}{\partial r} = J_W,$$
$$J_A = 0.$$

The vapor and air concentrations are calculated as

$$C_W(L,t) = \frac{P_W(t)}{RT_0}, \quad C_A(L,t) = \frac{P_A(t)}{RT_0}.$$

(e) Local temperature and vapor partial pressure inside the grain can be calculated from the state equation.

(f) We assumed the local adsorption equilibrium inside the grain so that the adsorption uptake $N(r, t)$ depends on the temperature and the partial vapor pressure and can be expressed as a universal function $N(F)$ presented in [8], where $F = RT \ln \frac{P_s(T)}{P}$.

The total balance of the water mass in the whole set-up is given by the following equation:

$$\frac{P_W(t)V}{RT_0} + m(t) = \frac{P_W(0)V}{RT_0} + m(0), \quad (4)$$

where V is the total volume of the gas phase in the set-up, $m(t)$ is the number of water moles in the adsorbed state. Eq. (4) was used to check the correctness of the numerical procedure.

5. Numerical results and discussion

5.1. Variable parameters

Eqs. (1)–(4) were numerically solved to calculate the dependences $P_w(t)$, $N(r, t)$, $C_w(z, t)$ and $T(r, t)$. As the function $N(F)$ is strongly non-linear, it asked for using iteration procedures which significantly increased the computation time. Variable parameters were the effective diffusivity D_W, the effective heat transfer coefficient α_p and the characteristic diffusional length L, which represents a spatial scale of the vapor concentration gradient. We determined these parameters using the following procedure: for each set (D_W, α_p and L) the average squared error σ of calculating the total pressure ($P_W + P_a$) was found, and its value was minimized. Fig. 3 gives the example of this calculation at $P_a = 1$ mbar, $L = 1.0$ m and various D_W and α_p. Similar graphs were plotted for various values of L. For the partial pressure of residual air at $P_a = 1$ mbar the minimal value of the error σ was found to reach at $L = 1.0$ M, $\alpha_p = 4.0$ W/(m^2 K) and $D_W = 3.1 \times 10^{-6}$ m^2/s that gives a good agreement between the experimental and calculated evolution of the total pressure (Fig. 4). In the similar way the analysis at other P_a was performed (see Table 1). Table 1 demonstrates that the length scale of changing the vapor and air (hydrogen) concentration is 1.0 M for all the experiments in the presence of residual gas. The effective diffusivity and heat transfer coefficients in pure vapor well agree with those obtained in the previous papers [8].

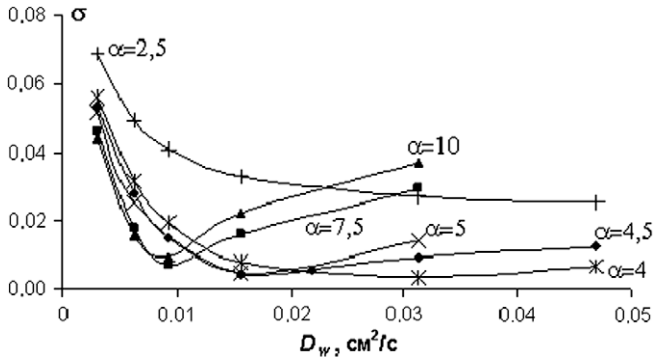

Fig. 3. Average squared error σ of calculating the vapor partial pressure P_w as a function of the vapor effective diffusivity at $L = 1.0$ M. $P_a = 1$ mbar and various α_p.

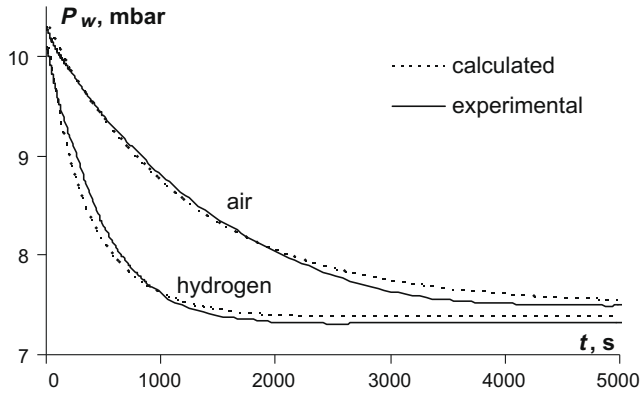

Fig. 4. Experimental [8] and calculated values of the total pressure over the adsorbent as a function of the adsorption time at the partial pressure of residual air and hydrogen of 1 mbar.

Table 1
Optimal values of the variable parameters at different partial pressures P_A of residual air and hydrogen.

P_A (mbar)	L (cm)	α_p (W/(m^2 K))	$D_W \cdot 10^6$ (m^2/s)
Air, 0	0.001	55	4.7
Air, 0.37	100	7.5	3.1
Air, 1.0	100	4	3.1
Air, 4.8	100	1.25	3.1
Air,14.3	110	0.5	3.1
H_2, 0.37	100	50	3.1
H_2, 1.0	100	25	3.1
H_2, 4.5	100	4	3.1
H_2, 14.3	100	1.5	3.1

5.2. Effective heat transfer coefficient

Table 1 and Fig. 5 clearly show that the heat transfer coefficient reduces in the presence of residual gas (air or hydrogen) that is in agreement with the literature data presenting similar decrease during vapor condensation [15,16]. Indeed, typical value of the effective coefficient of heat transfer in a pure vapor $\alpha_p = 50$–70 W/(m^2 K) [8] dramatically drops even at a little admixture of air, e.g. only 4 W/(m^2 K) at $P_a = 1.0$ mbar or $P_a/P_W = 0.097$. Reduction of the heat transfer coefficient is less dramatic in the presence of hydrogen that is due to its large diffusivity which favors destroying the gas-reach layer as discussed above.

5.3. Effective water diffusivity

Despite of the residual gas pressure, the effective diffusivity of water inside the SWS pores is constant and equal to $3.1 \times$

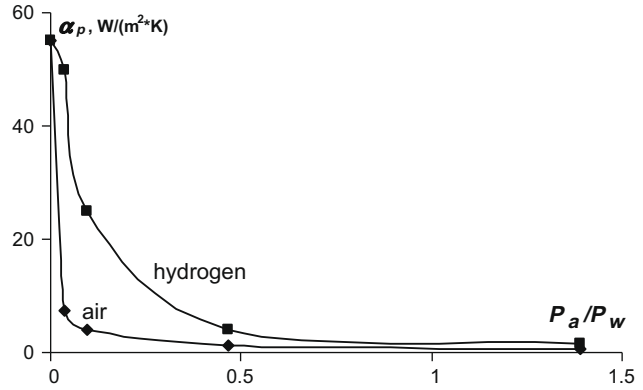

Fig. 5. Effective coefficient of heat transfer as a function of the ratio P_a/P_W.

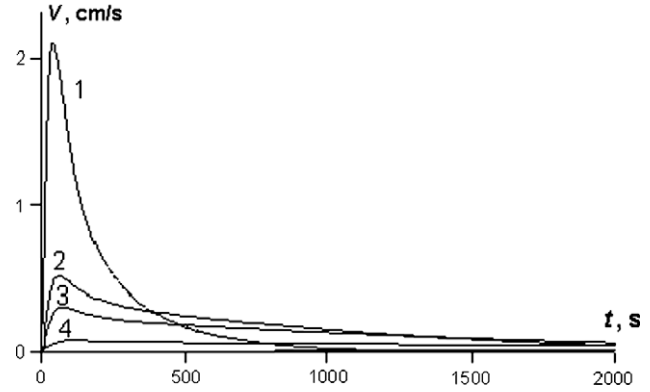

Fig. 6. Velocity of the convective vapor flux near the grain surface at various air pressure P_a: 1 – 0.37; 2 – 1; 3 – 4.8; and 4 – 14.3.

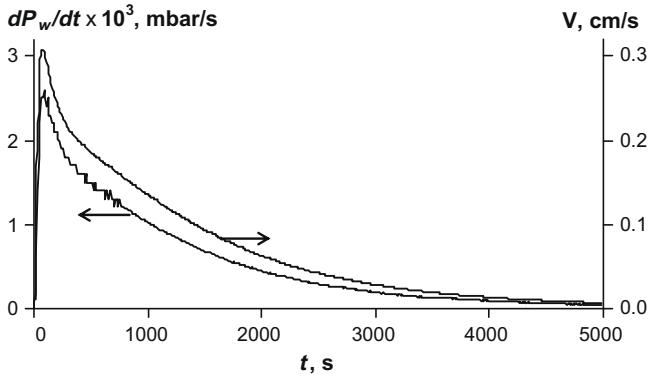

Fig. 8. Temporal evolution of the velocity of convective air flux near the grain surface (1) and the rate of vapor adsorption (2). Partial air pressure P_a = 1 mbar.

10^{-6} m^2/s. This value indicates that the mechanism of water transport inside the pores is likely to be the Knudsen diffusion. Indeed, the average pore diameter of SWS-1L $d_{av} = 2r_p = 15$ nm is much smaller that the mean free path (l) of water molecules at $T = 60$ °C and $P_{H_2O} = 10$ mbar, $l = \frac{kT}{\pi P \sigma^2 \sqrt{2}} = 8570$ nm, where σ is the effective diameter of a water molecule. As $d_{av} \ll l$, one can expect the Knudsen diffusion mechanism with the water diffusivity [17] $D_{kn} = 9700 r_p \sqrt{T/M} = 3.0 \times 10^{-6}$ m^2/s, that is in a good agreement with the effective diffusivities presented in Table 1.

5.4. Dynamics of water adsorption in the presence of residual air

In the absence of a residual gas the quick cooling of the metal support (and owing to it of the adsorbent grains) initiates adsorption of water by the grain. Adsorption of pure vapor is generally controlled by surface or/and intraparticle heat and mass transfer resistance. Because of the irreversible adsorption, a convective flux of vapor towards the grain external surface is formed. The velocity of this flux depends on the adsorption rate and passes through the maximum at the adsorption time of 70 s (Fig. 6). At longer times it reduces as the sorption rate is going down.

As mentioned above, the sorption rate may significantly decrease in the presence of air due to the effective air sweeping to the grain surface where it is accumulated as an air-rich layer. Fig. 7 demonstrates the formation and temporal evolution of this layer at P_a = 1 mbar. At the beginning of the adsorption process, the partial pressure of air near the grain external surface increases with respect to its initial pressure by some 1.5–2.5 mbar. After passing the maximum, it gradually reduces down to the initial value (Fig. 7). The partial pressure of vapor changes accordingly. Both the formation and the decay of the air-rich layer are faster at lower air pressure P_a. For SWS-1L a typical time for the formation of air-reach layer is 150 s at P_a = 0.37 mbar, 300 s at P_a = 1 mbar and 600 s at P_a = 4.8 mbar. If the water sorption equilibrium is reached faster than this time, the layer is underdeveloped and the effect of residual air is less dramatic. Indeed, the residual air more strongly affects adsorption on SWS-1L with larger equilibrium uptake than on the microporous silica Fuji RD [8]. The formation of the air-rich layer significantly reduces the transfer of vapor to the surface as it is now controlled by the vapor diffusion through this layer which is relatively slow compared with adsorption process inside the grain. Indeed, the velocity of the convective vapor flux near the grain surface drastically falls when the air pressure increases (Fig. 8).

The initial and final radial distributions of the adsorbed water are homogeneous and correspond to N = 2.1 and 4.5 mole/mole, respectively (Fig. 9). At intermediate times, a higher concentration is observed near the external grain surface.

6. Conclusions

New experimental data on the kinetics of water vapor adsorption on the loose grains of SWS-1L under real conditions of AHT in the presence of residual hydrogen have been obtained by the Large Temperature Jump method. The data are used to assess the comparative impact of residual hydrogen and air on the sorption dynamics. Effects of air and hydrogen, being admixed to water vapor at the partial pressure P_A, are found to exhibit a remarkable similarity:

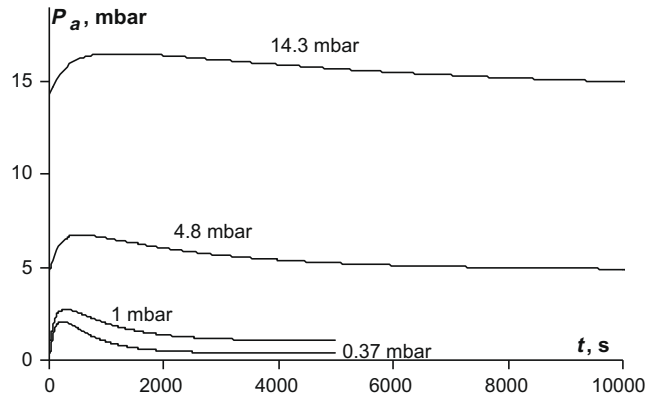

Fig. 7. Partial pressure of air near the external grain surface as a function of time at various air pressure.

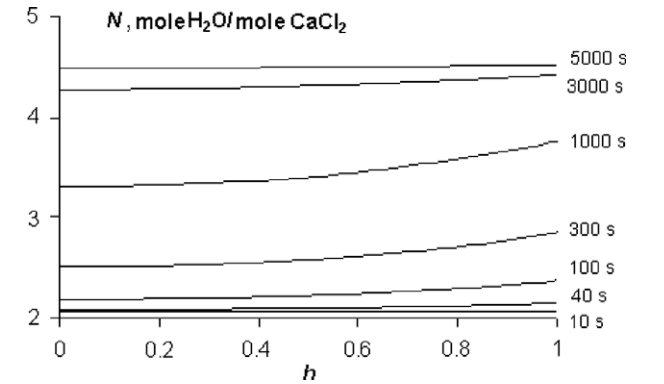

Fig. 9. Profiles of adsorbed water vs. the dimensionless radius of the grain at various adsorption time.

– at any P_A, the kinetic curves of water sorption are near-exponential over the whole range of uptake;
– the characteristic time of sorption increases as $\tau = \tau_0 + BP_A$ because of significant slowing down the sorption of water;
– this rate reduction is caused by a Stephan flux which effectively sweeps gas to the adsorbent surface where it is accumulated as a gas-rich layer.

Larger diffusivity of hydrogen results in an important quantitative difference between the two gases: the ratio of the slopes $B(\text{air})/B(H_2) = 3.64$ demonstrates that the effect of residual hydrogen is less dramatic as compared with air. Indeed, the Stephan flux driven by the water sorption strives to separate the gas and vapor, while the diffusion promotes their mixing. Disordering tendency is more efficient for a lighter gas (hydrogen).

To take into account these randomizing and ordering processes, a new mathematical model of the coupled heat and mass transfer in an adsorbent layer has been developed. This model describes the origin of the Stephan flux, the formation and temporal evolution of the gas-rich layer near the surface of the composite sorbent SWS-1L. Basic information was obtained by calculating the temperature, pressure and concentration of the adsorbed water as a function of time. Variable parameters (the effective diffusivity, the effective heat transfer coefficient and the characteristic scale of vapor concentration gradient) have been assessed by fitting calculated dependences of the total pressure over the adsorbent to the experimental ones:

– a typical scale of the gas gradient concentration is found to be 1 m;
– the effective diffusivity is close to the estimated Knudsen diffusivity inside the pores that is in good agreement with the literature data;
– the effective coefficient of heat transfer, which is equal to 50–70 $W/(m^2\,K)$ in a pure vapor, dramatically drops even at a little admixture of air, e.g. only 4 $W/(m^2\,K)$ at $P_a = 1.0$ mbar or $P_a/P_W = 0.097$.

Because of the irreversible adsorption a convective (Stephan) flux of vapor towards the grain external surface is formed. The linear velocity of this flux depends on the adsorption rate and passes through the maximum at the adsorption time approximately 70 s. At longer times it reduces as the sorption rate is going down. This vapor flux carries the gas molecules towards the grain external surface where the gas partial pressure increases with respect to its initial pressure by some 1.5–2.5 mbar. After passing the maximum, it gradually reduces down to the initial value. For SWS-1L, a typical time for the formation of air-reach layer is 150 s at $P_a = 0.37$ mbar, 300 s at $P_a = 1$ mbar and 600 s at $P_a = 4.8$ mbar. If the water sorption equilibrium is reached faster than this time, the layer is underdeveloped and the effect of residual air is less dramatic. Another reason for underdevelopment of the layer is restricted number of gas molecules in the system, which has not been taken into account in the model involved (see Appendix A).

Acknowledgments

The authors thank the Russian Foundation for Basic Researches (Projects 08-08-90016 and 08-08-00808) for partial financial support.

Appendix A

Special feature of the LTJ experiment [8] is the presence of a vapor vessel of large volume ($V_{VV} = 30.5 \times 10^{-3}\ m^3$) linked to a measuring cell of small volume ($V_{MC} = 0.14 \times 10^{-3}\ m^3$) where the adsorbent grains (0.420–0.425 g) are located covering a circle of the area $S = 9.1\ cm^2$. This vessel is used to moderate the vapor pressure change in the constant volume caused by adsorption and make this process as quasi-isobaric. At the gas pressure $P_A = 1.0$ mbar, this vessel contains $n = (P_A \cdot V_{VV})/(R \cdot T) = (100\ Pa \cdot 30.5 \times 10^{-3}\ m^3)/(8.314\ J/mol/K \cdot 333\ K) = 1.1 \times 10^{-3}$ mole of the gas or 6.7×10^{20} molecules. The maximum resistance for vapor transfer would be if all these gas molecules are located in the volume $V = nRT/P = (1.1 \times 10^{-3}\ mol)\,(8.314\ J/mol/K \cdot 308\ K)/(1000\ Pa) = 2.8 \times 10^3\ cm^3$ near the surface of the adsorbent layer (at $P = 10$ mbar) to form the gas-rich layer of the thickness $\Delta z = 6.2$ m (at total pressure 10 mbar) with the constant concentration gradient $\Delta C/\Delta z = (0.39\ mol/m^3)/(6.2\ m) = 0.063\ mol/m^4 = 6.3 \times 10^{-10}\ mol/cm^4$. This estimation confirms that the typical space scale of the vapor concentration gradient is 1 m. The vapor diffuses towards the adsorbent surface, and the flux can be estimated as $J = -DS\Delta C/\Delta z = (29.2\ cm^2/s)\,(9.1\ cm^2)\,(6.3 \times 10^{-10}\ mol/cm^4) = 1.7 \times 10^{-7}$ mol/s. This flux can be compared with the maximum rate of pure vapor sorption ($P_A = 0$): under the conditions fixed in this work, the characteristic time of water sorption by a monolayer of SWS-1L loose grain is $\tau = 200$ s (Fig. 1). Hence, the specific adsorption rate of pure vapor is $\Delta q/(\tau\mu_w) = (0.14\ g/g)/(300\ s)/(18\ g/mol) = 3.9 \times 10^{-5}$ mol/s, where Δq is the amount of water adsorbed by 1 g of the adsorbent. This is approximately 200 times larger than the flux estimated above which presents the sorption rate when all air would be collected from the vessel and accumulated near the grain surface. As seen from Fig. 2, in our LTJ runs the adsorption rate was reduced by a factor of 5 and 2 for 1 mbar of air and hydrogen, respectively.

In general, the total volume of non-adsorbable gas V in a real AHT depends on its residual pressure P_A and a "dead volume" V_d which represents a volume available for the gas and vapor: $V_A = V_d[P_A/(P_A + P_W)] = V_d\delta$, where $\delta = P_A/(P_A + P_W)$ is a relative content of the residual gas. If all this gas were accumulated near the surface S of the vapor transfer, it would form the layer of the thickness $\Delta z = V_A/S = \delta(V_d/S)$. If the dead volume is small and the surface S is large, the thickness of the gas-rich layer is small. Its diffusional resistance is small as well. Appropriate concentration gradient is $\Delta C/(2\Delta z) = [(P_A + P_W)/RT]/[2\delta(V_d/S)]$, and the diffusional flux $J = -DS\Delta C/\Delta z = [D_0/(P_A + P_W)]S(P_A + P_W)/(RT)/[2\delta(V_d/S)] = D_0S^2/(RT)/[2\delta(V_d)]$ most strongly depends on the mass transfer surface S, while it does not depend on the total pressure ($P_A + P_W$). Hence, to reduce the influence of the residual gas it is necessary first of all to develop the mass transfer surface as well as to decrease the gas content and the dead volume of the AHT unit.

References

[1] F. Meunier, Solid sorption: an alternative to CFCs, Heat Recovery Syst. CHP 13 (4) (1993) 289–295.
[2] R.Z. Wang, R.G. Oliveira, Adsorption refrigeration – an efficient way to make good use of waste heat and solar energy, Prog. Energy Combust. Sci. 32 (2006) 424–458.
[3] R.E. Critoph, Y. Zhong, Review of trends in solid sorption refrigeration and heat pumping technology, J. Process Mech. Eng. E 219 (3) (2005) 285–300.
[4] F. Ziegler, Recent developments and future prospects of sorption heat pump systems, Int. J. Therm. Sci. 38 (1999) 91–208.
[5] V.P. Vorotilin, L.I. Heifets, Chemical Industry 8 (1987) 502–506 (in Russian).
[6] D.A. Frank-Kamenetskiy, Diffusion and Heat Transfer in Chemical Kinetics, Nauka, Moscow, 1967. pp. 57–140.
[7] L.I. Heifets, D.M. Predtechenskaya, Yu.V. Pavlov, B.N. Okunev, Modeling of the dynamic effects in the adsorbent beds. Part 1. Simple method of estimation of thermal conductivity of the composite adsorbent bed ($CaCl_2$ impregnated into pores of silica gel lattice), Vestnik MGU Ser. 2, 47(4) (2006) 274–277.
[8] I.S. Glaznev, Yu.I. Aristov, Kinetics of water adsorption on loose grains of SWS-1L under isobaric stages of adsorption heat pumps: the effect of residual air, Int. J. Heat Mass Transfer 51 (25–26) (2008) 5823–5827.
[9] I.S. Glaznev, D.S. Ovoshchnikov, Yu.I. Aristov, Dynamics of water adsorption on loose grains in the presence of non-adsorbable gas under typical operating conditions of an adsorptive chiller, cryogenics and refrigeration. Proc. ICCR'2008, Shanghai, China, April 5–9, 2008, pp. 570–574.

[10] B.N. Okunev, A.P. Gromov, L.I. Heifets, Yu.I. Aristov, A new methodology of studying the dynamics of water sorption/desorption under real operating conditions of adsorption heat pumps: modelling of coupled heat and mass transfer, Int. J. Heat Mass Transfer 51 (2008) 246–252.
[11] Yu.I. Aristov, B. Dawoud, I.S. Glaznev, A. Elyas, A new methodology of studying the dynamics of water sorption/desorption under real operating conditions of adsorption heat pumps: experiment, Int. J. Heat Mass Transfer 51 (19–20) (2008) 4966–4972.
[12] T.K. Sherwood, R.L. Pigford, C.R. Wilkel, Mass Transfer, McGraw-Hill, New York, 1975. pp. 29–43.
[13] Yu.I. Aristov, M.M. Tokarev, G. Cacciola, G. Restuccia, Specific heat and thermal conductivity of aqueous solutions of calcium chloride in silica pores, Russ. J. Phys. Chem. 71 (3) (1997) 391–394.
[14] M.M. Tokarev, B.N. Okunev, M.S. Safonov, L.I. Heifets, Yu.I. Aristov, Approximation equations for describing the sorption equilibrium between water vapor and a $CaCl_2$-in-silica gel composite sorbent, Russ. J. Phys. Chem. 79 (9) (2005) 1490–1494.
[15] S.S. Kutateladze, Fundamentals of Heat Transfer, Academic Press, New York, 1963. pp. 406–407.
[16] H.A. Hasanein, M.S. Kazimi, M.W. Golay, Forced convection in-tube condensation in presence of non-condensable gases, Int. J. Heat Mass Transfer 39 (13) (1996) 2625–2639.
[17] L.I. Heifets, A.V. Neimark, Multiphase Processes in Porous Media, Khimiya, Moscow, 1982 (in Russian).